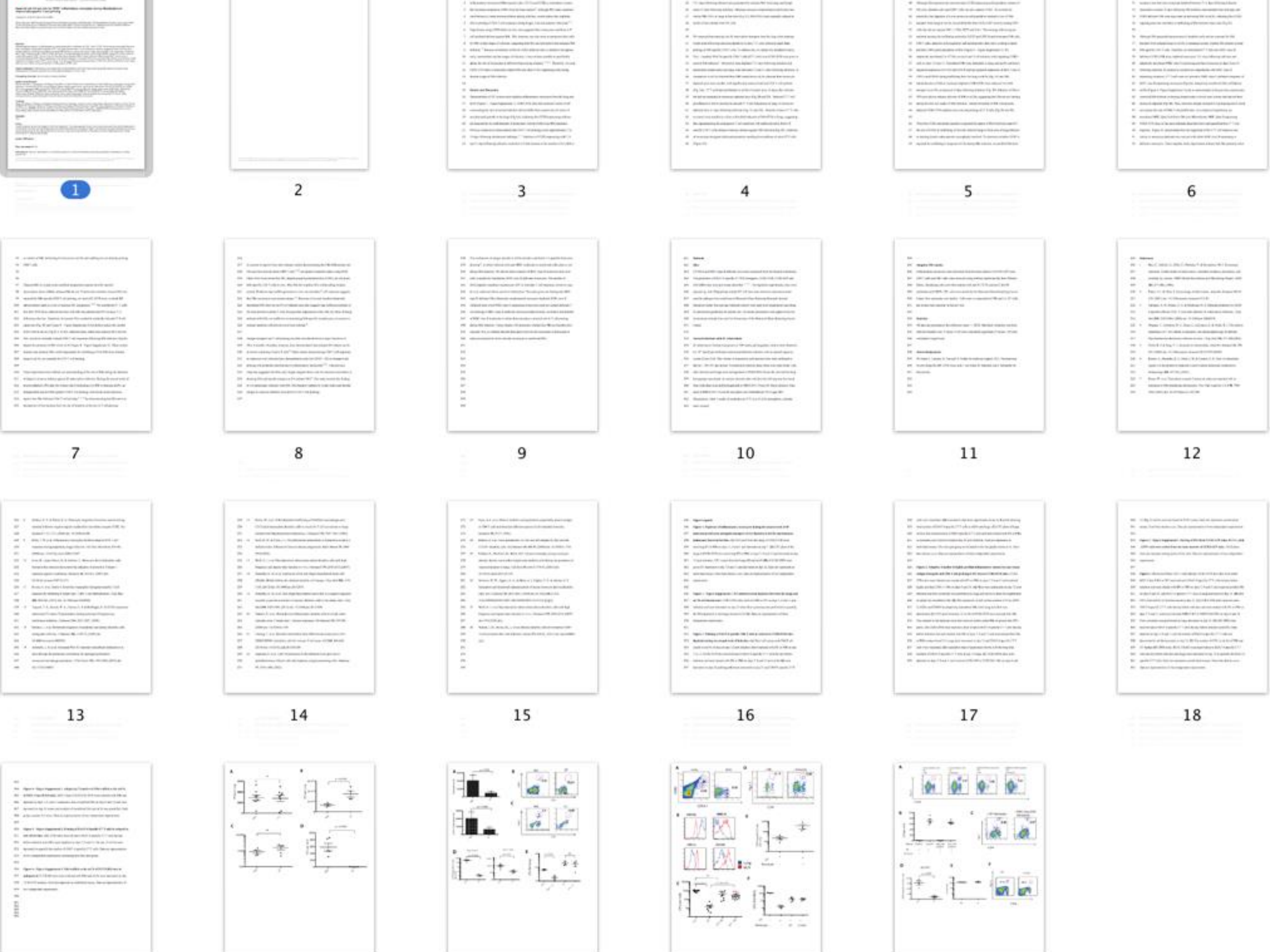
1
2
3
4
5
6
7
8
9
10
11
12
13
14
15
16
17
18

Ivan Grubisic

Concept, prototype testing, development

Michael Aufreiter

front end, javascript, interface, development

Graham Nott

xml workflows and back end, image processing

A DNA Repair Complex Functions as an Oct4/Sox2 Coactivator in Embryonic Stem Cells

Yick W. Fong, Carla Inouye, Teppei Yamaguchi, Claudia Cattoglio, Ivan Grubisic, Robert Tjian

unambiguously and systematically test and identify transcriptional cofactors that may be directly required to potentiate Oct4- and Sox2-dependent gene activation of *Nanog*. Here, we report the biochemical purification and identification of a multisubunit stem cell coactivator (SCC) that is required for the synergistic activation o *Nanog* by Oct4 and Sox2 in vitro. After extensive biochemical characterization, we surprisingly found that SCC is none other than the XPC-RAD23B-CETN2 (XPC) nucleotide excision repair (NER) complex. SCC/XPC interacts directly with Oct4 and Sox2 and co-occupies a majority of Oct4 and Sox2 targets genome-wide in mouse ES cells. Importantly, SCC/XPC is required for stem cell self-renewal and efficient somatic cell reprogramming. Thus, our findings unmask an unanticipated selective coactivator role of an NER complex in transcription in the context of ES cells and may provide a previously unknown molecular link that couples stem cell-specific transcription to DNA damage response with potential implications for enhanced ES cell genome stability.

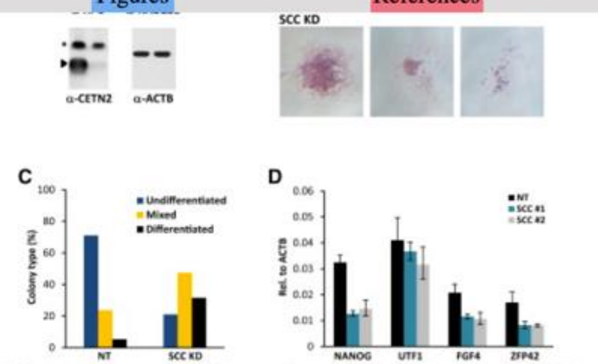

Figure 5. SCC Is Required for ES Cell Maintenance(A) Efficiency of shRNA-mediated depletion of SCC in
Whole-cell extracts of mouse D3 cells infected with nontarget (NT) lentiviruses (MOI of 300) or with an equ
lentiviruses (MOI of 100 each) targeting XPC, RAD23B, and CETN2 (SCC KD) are analyzed by western bl
recognized by their respective antibodies are indicated by filled arrowheads. Asterisks denote nonspecific sig
morphology and alkaline phosphatase (AP) activity (red) are maintained in control D3 cells (NT, top) but are
SCC-depleted D3 cells (SCC KD, bottom). See also Figure S4C.(C) Clonal assays on SCC-depleted D3 ES c
and SCC-depleted (SCC KD) D3 cell pools were plated at 300 cells per well in 6-well plates, and emerging c
activity. Differentiation status was scored based on AP staining intensity, ES cell morphology, and colony int
nonoverlapping sets of shRNAs targeting SCC (SCC #1 and SCC #2) are used to deplete SCC. Quantificatio
Zfp42 mRNA levels are analyzed by real-time quantitative PCR (qPCR) and normalized to *Actb*. Data from r
are shown; error bars represent standard deviations. n = 3.See also Figure S4.

Results

Detection of an Oct4- and Sox2-Dependent Coactivator Activity in EC and ES Cells

Having chosen the *Nanog* promoter as our model template, we next set out to develop an in vitro reconstitutec transcription assay that could recapitulate the Oct4- and Sox2-dependent transactivation at the *Nanog* promote observed in vivo. To enhance the sensitivity of the assay, we inserted four copies of the *Nanog* oct-sox-bindin sites immediately upstream of the native oct-sox element found in the human *Nanog* promoter. Our basal in vitro transcription assay consisted of purified recombinant TFIIA, -B, -E and -F together with immunoaffinity-purified native RNA polymerase II, TFIID, and TFIIH (Figure S1A available online). When purified Oct4 and Sox2 were added to this reconstituted transcription system, only a very weak activation of the *Nanog* promoter was detected (Figure 1A, lanes 1 and 2). As a control, we could show that the same complement of general transcription factors (GTFs) was able to support strong Sp1-dependent activation from a GC box-containing "generic" transcription template (G3BCAT) (Figure 1A, lanes 5 and 6). This initial resul suggested that efficient activation of *Nanog* by Oct4 and Sox2 may require additional cofactors to potentiate a full activator-dependent response.

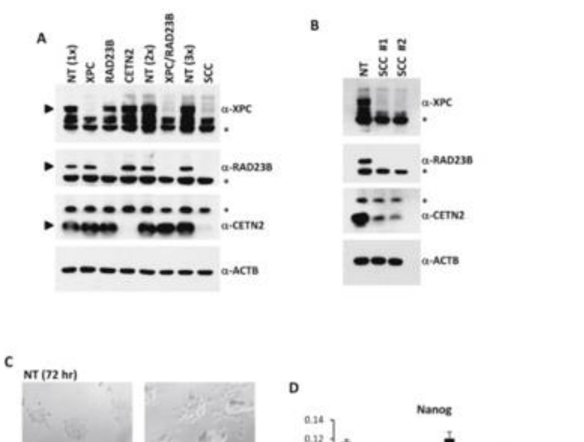

We reasoned that such a putative coactivator ought to be selectively active in pluripotent cell types that expres Nanog under the control of Oct4 and Sox2. For example, NTERA-2 (NT2) is a pluripotent human embryonal carcinoma (EC) cell line that expresses Oct4, Sox2, and Nanog and shares with ES cells core molecular mechanisms that govern self-renewal (Pal and Ravindran, 2006). Detailed expression profiling of NT2 and bona fide human ES cell lines revealed many similarities, including robust expression of Nanog (Schwartz et al., 2005 and Sperger et al., 2003). However, unlike human ES cells, NT2 cell culture can be more readily scaled up, a prerequisite to generating sufficient quantities of starting materials for the biochemical purificatio of putative Oct4/Sox2 coactivators. We therefore chose extracts derived from NT2 cells as our starting materi

Contents Figures References Article Info

A longitudinal study of Caenorhabditis elegans larvae reveals a novel locomotion switch, regulated by Gαs signaling

Stanislav Nagy Charles Wright Nora Tramm
Nicholas Labello Stanislav Burov David Biron

Abstract

Despite their simplicity, longitudinal studies of invertebrate models are rare. We thus sought to characterize behavioral trends of *Caenorhabditis elegans*, from the mid fourth larval stage through the mid young adult stage. We found that, outside of lethargus, animals exhibited abrupt switching between two distinct behavioral states: active wakefulness and quiet wakefulness. The durations of epochs of active wakefulness exhibited non-Poisson statistics. Increased $G_{\alpha s}$ signaling stabilized the active wakefulness state before, during and after lethargus. In contrast, decreased $G_{\alpha s}$ signaling, decreased neuropeptide release, or decreased CREB activity destabilized active wakefulness outside of, but not during, lethargus. Taken together, our findings support a model in which protein kinase A

Figure 3.

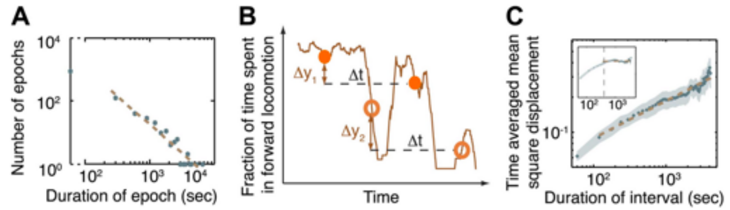

The dynamics of the active wakefulness state during the three hours prior to L4 lethargus in wild-type animals.

(**A**) A histogram of the durations of epochs of active wakefulness plotted on a log-log scale. Epoch durations longer than 3 min exhibited a power-law distribution with an exponent $-(1+\alpha) = -1.83\pm0.31$. (**B**) Two displacements along the y-axis of a sample trace of the fraction of forward locomotion, Δy_1 (between filled circles) and Δy_2 (between empty circles). Both displacements correspond to an identical time interval, Δt. The time-averaged mean square displacement (TMSD) is calculated in two steps: (i) using a sliding window to calculate the mean squared displacements along traces of each of the individual animals (Golding and Cox, 2006); (ii) averaging the results obtained from the previous step for all animals. (**C**) The TMSD plotted on a log-log scale as a function of the time-interval, Δt. The TMSD was calculated for the subset of N = 20 animals where data 3 hr prior to the onset of L4leth was available (N = 20). The TMSD exhibited power-law growth with the exponent $(1-\alpha) = 0.32 \pm 0.03$, consistent with a value of $\alpha \approx 0.7$. Inset: for the purpose of illustration, the TMSD for a two-state Markov chain with a comparable mean duration of epochs is shown to reach its saturation value at $\Delta t \approx 400$ s (vertical dashed line).

DOI: http://dx.doi.org/10.7554/eLife.00782.005

Figure 4.

0.2.0

stm

Contents Figures References Article Info

A longitudinal study of Caenorhabditis elegans larvae reveals a novel locomotion switch, regulated by Gαs signaling

Stanislav Nagy Charles Wright Nora Tramm
Nicholas Labello Stanislav Burov David Biron

Abstract

Despite their simplicity, longitudinal studies of invertebrate models are rare. We thus sought to characterize behavioral trends of *Caenorhabditis elegans*, from the mid fourth larval stage through the mid young adult stage. We found that, outside of lethargus, animals exhibited abrupt switching between two distinct behavioral states: active wakefulness and quiet wakefulness. The durations of epochs of active wakefulness exhibited non-Poisson statistics. Increased $G_{\alpha s}$ signaling stabilized the active wakefulness state before, during and after lethargus. In contrast, decreased $G_{\alpha s}$ signaling, decreased neuropeptide release, or decreased CREB activity destabilized active wakefulness outside of, but not during, lethargus. Taken together, our findings support a model in which protein kinase A

Figure 3.

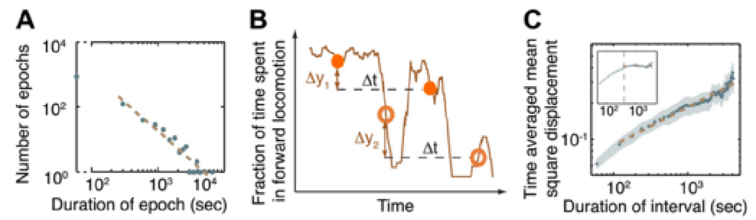

The dynamics of the active wakefulness state during the three hours prior to L4 lethargus in wild-type animals.

(**A**) A histogram of the durations of epochs of active wakefulness plotted on a log-log scale. Epoch durations longer than 3 min exhibited a power-law distribution with an exponent $-(1+\alpha) = -1.83 \pm 0.31$. (**B**) Two displacements along the y-axis of a sample trace of the fraction of forward locomotion, Δy_1 (between filled circles) and Δy_2 (between empty circles). Both displacements correspond to an identical time interval, Δt. The time-averaged mean square displacement (TMSD) is calculated in two steps: (i) using a sliding window to calculate the mean squared displacements along traces of each of the individual animals (Golding and Cox, 2006); (ii) averaging the results obtained from the previous step for all animals. (**C**) The TMSD plotted on a log-log scale as a function of the time-interval, Δt. The TMSD was calculated for the subset of N = 20 animals where data 3 hr prior to the onset of L4leth was available (N = 20). The TMSD exhibited power-law growth with the exponent $(1-\alpha) = 0.32 \pm 0.03$, consistent with a value of $\alpha \approx 0.7$. Inset: for the purpose of illustration, the TMSD for a two-state Markov chain with a comparable mean duration of epochs is shown to reach its saturation value at $\Delta t \approx 400$ s (vertical dashed line).

DOI: http://dx.doi.org/10.7554/eLife.00782.005

Figure 4.

stm

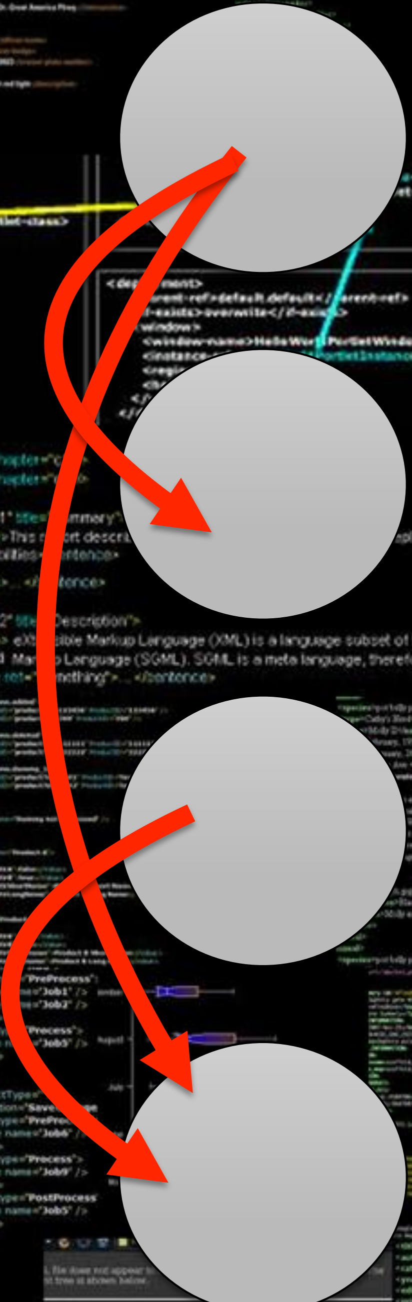

In NLM XML most links are one-way

```
      1
    ]
  },
  "text:59": {
    "type": "text",
    "id": "text:59",
    "content": "where GDP′ is GDP linearized on a scale of 0
  },
  "annotation:60": {
    "type": "figure_reference",
    "id": "annotation:60",
    "source": "text:59",
    "target": "image:fig1",
    "key": "content",
    "content": "Figure 1A",
    "pos": [
      51,
      9
    ]
  },
  "annotation:61": {
    "type": "publication_reference",
    "id": "annotation:61",
    "source": "text:59"
```


In Lens JSON we make two-way links explicit

Lens V0.1

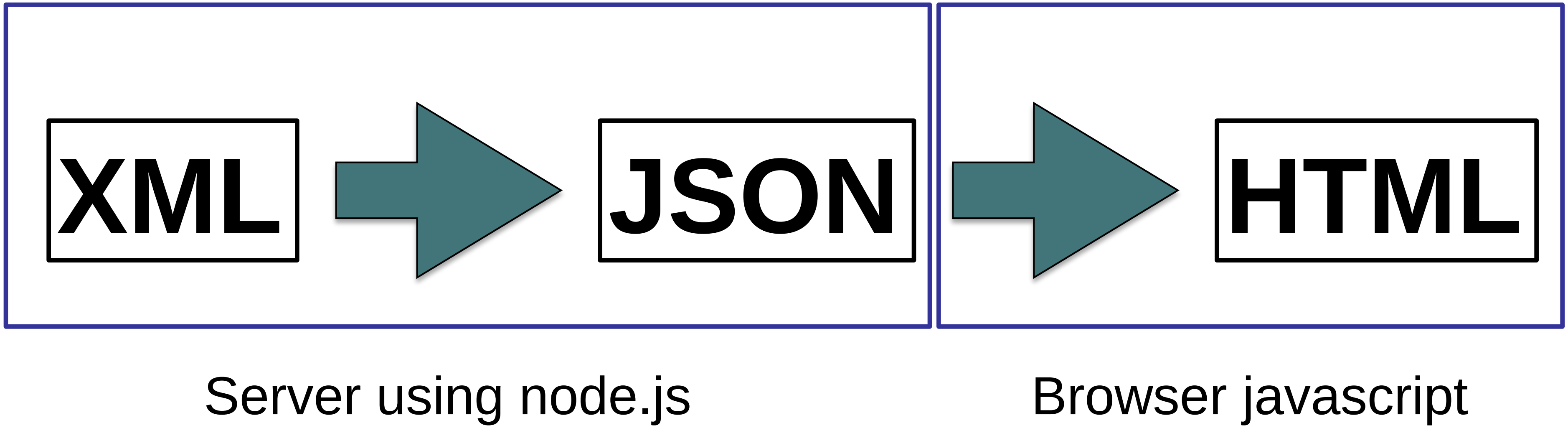

Lens V0.2

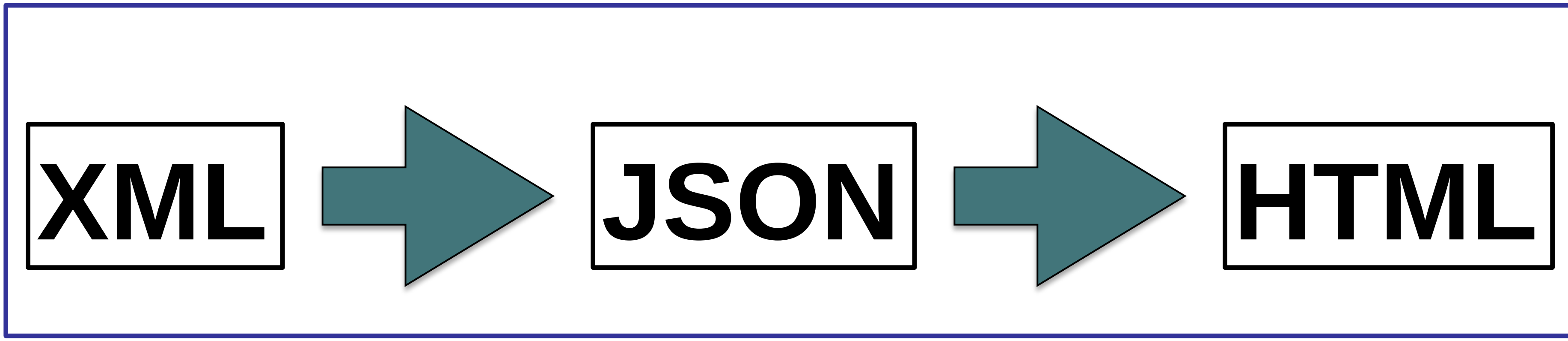

Put ALL THE THINGS IN THE Browser javascript

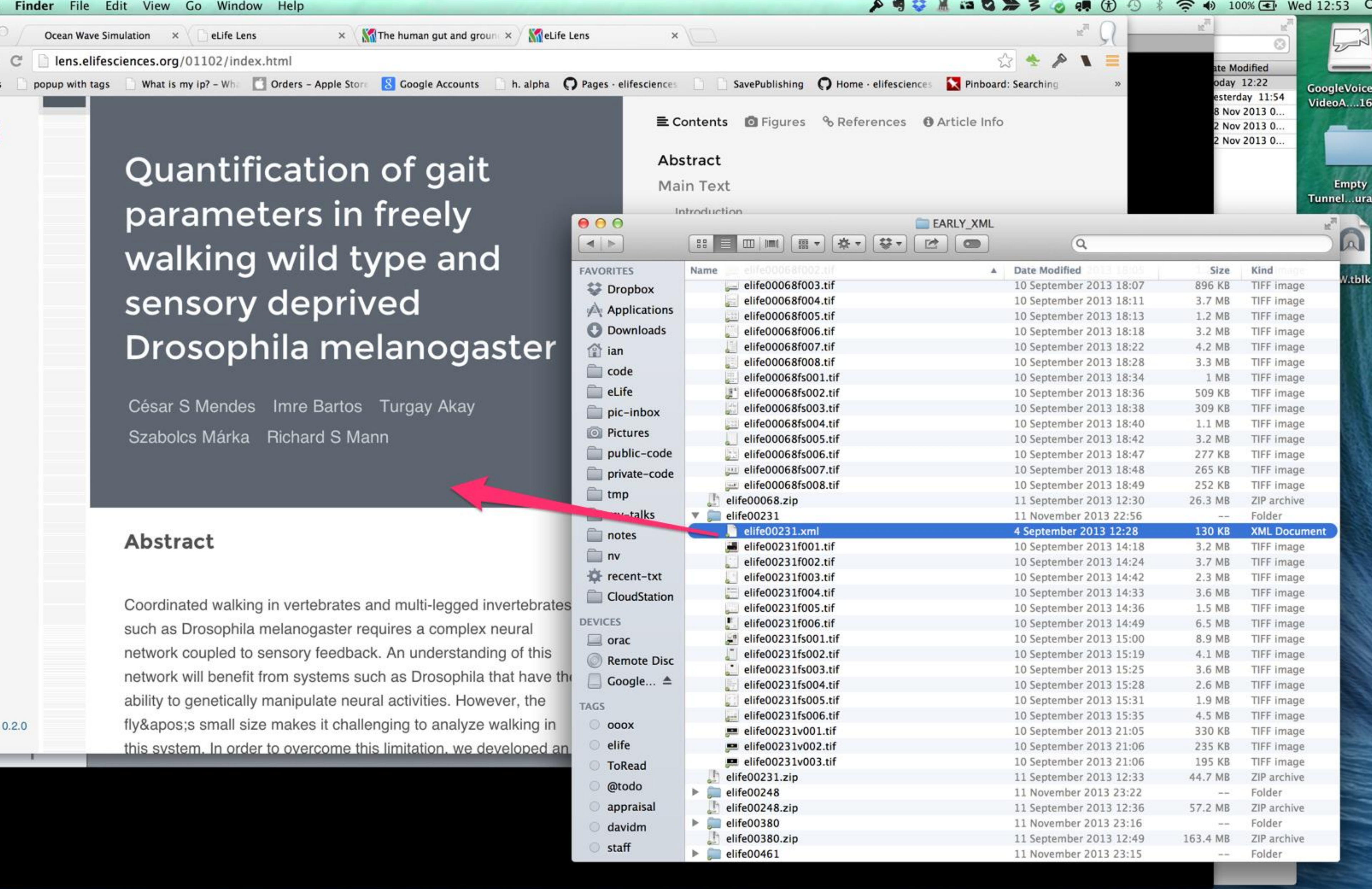
Finder File Edit View Go Window Help
Wed 12:53
Ocean Wave Simulation
eLife Lens
The human gut and groun
eLife Lens
lens.elifesciences.org/01102/index.html
Quantification of gait parameters in freely walking wild type and sensory deprived Drosophila melanogaster
César S Mendes Imre Bartos Turgay Akay Szabolcs Márka Richard S Mann
Abstract
Coordinated walking in vertebrates and multi-legged invertebrates such as Drosophila melanogaster requires a complex neural network coupled to sensory feedback. An understanding of this network will benefit from systems such as Drosophila that have th ability to genetically manipulate neural activities. However, the fly's small size makes it challenging to analyze walking in this system. In order to overcome this limitation, we developed an
Contents Figures References Article Info
Abstract
Main Text
EARLY_XML
FAVORITES
Dropbox
Applications
Downloads
DEVICES
TAGS
Name
Date Modified
Size
Kind
elife00231
elife00231.xml
4 September 2013 12:28
130 KB
XML Document
elife00231.zip
ZIP archive
Folder
TIFF image

stm

```
<html xmlns:mml="http://www.w3.org/1998/Math/MathML">
  <head>
    <title>eLife Lens</title>
    <link href='http://fonts.googleapis.com/css?family=Montserrat:400,700' rel='stylesheet' type='text/css'>
    <link href='../lens-elife/styles/font-awesome.css' rel='stylesheet' type='text/css'/>

    <link href='../lens-elife/lens.css' rel='stylesheet' type='text/css'/>

    <script src="../lens-elife/lib/jquery-2.0.3.min.js"></script>

    <!-- MathJax -->
    <script type="text/x-mathjax-config">
    MathJax.Hub.Config({
      "HTML-CSS": { linebreaks: { automatic: true } },
             SVG: { linebreaks: { automatic: true } }
   });
    </script>
    <script type="text/javascript" src="http://cdn.mathjax.org/mathjax/latest/MathJax.js?config=TeX-AMS-MML_HTMLorMML"></script>

    <script src='../lens-elife/lens.min.js'></script>

    <script>

      if (window.Lens === undefined) {
        window.Lens = require("/src/lens.js");
      }

      // Create a new Lens app instance
      // --------
      //
      // Injects itself into body

      var app = new Lens({
        // Endpoint must have CORS enabled, or file is served from the same domain as the app
        document_url: "https://s3.amazonaws.com/elife-cdn/elife-articles/01102/elife01102.xml"
        // document_url: "data/about/index.xml"
      });

      $(function() {
        app.start();
      });

    </script>

    <script src="../ga.js"></script>

  </head>
  <body>

  </body>
</html>
```

1 - Call the Javascript

2 - Point at an XML file

Lens V0.??

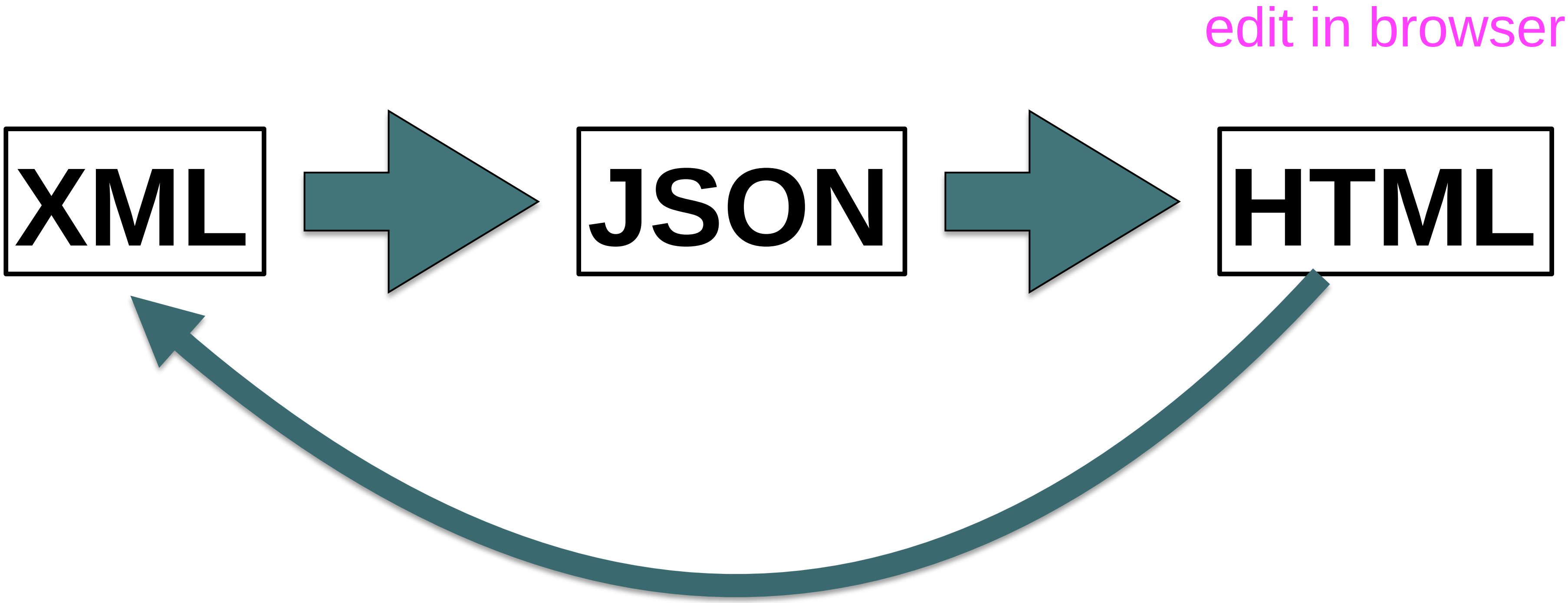

NOW

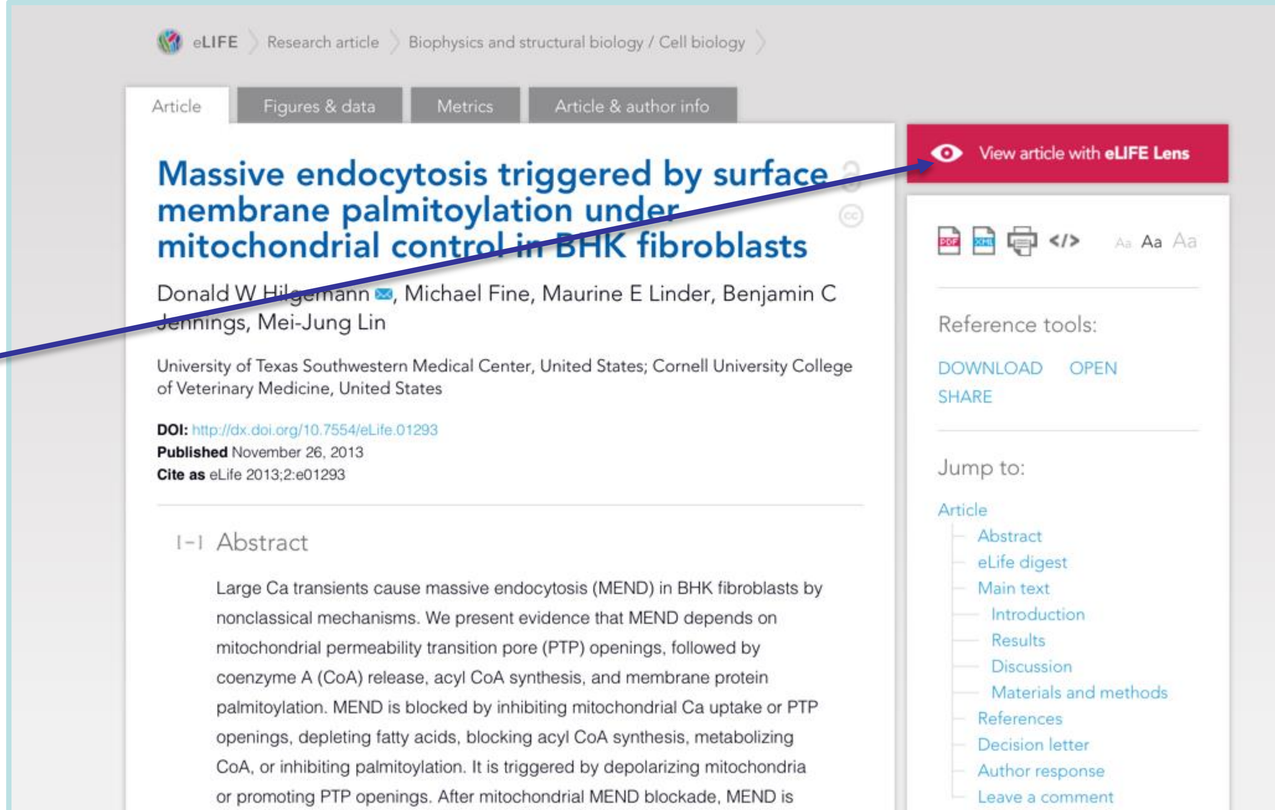

eLIFE › Research article › Biophysics and structural biology / Cell biology

Article | Figures & data | Metrics | Article & author info

View article with eLIFE Lens

Massive endocytosis triggered by surface membrane palmitoylation under mitochondrial control in BHK fibroblasts

Donald W Hilgemann, Michael Fine, Maurine E Linder, Benjamin C Jennings, Mei-Jung Lin

University of Texas Southwestern Medical Center, United States; Cornell University College of Veterinary Medicine, United States

DOI: http://dx.doi.org/10.7554/eLife.01293
Published November 26, 2013
Cite as eLife 2013;2:e01293

Reference tools:
DOWNLOAD OPEN SHARE

Jump to:

Article
- Abstract
- eLife digest
- Main text
  - Introduction
  - Results
  - Discussion
  - Materials and methods
- References
- Decision letter
- Author response
- Leave a comment

Abstract

Large Ca transients cause massive endocytosis (MEND) in BHK fibroblasts by nonclassical mechanisms. We present evidence that MEND depends on mitochondrial permeability transition pore (PTP) openings, followed by coenzyme A (CoA) release, acyl CoA synthesis, and membrane protein palmitoylation. MEND is blocked by inhibiting mitochondrial Ca uptake or PTP openings, depleting fatty acids, blocking acyl CoA synthesis, metabolizing CoA, or inhibiting palmitoylation. It is triggered by depolarizing mitochondria or promoting PTP openings. After mitochondrial MEND blockade, MEND is

NEXT → Peer Review

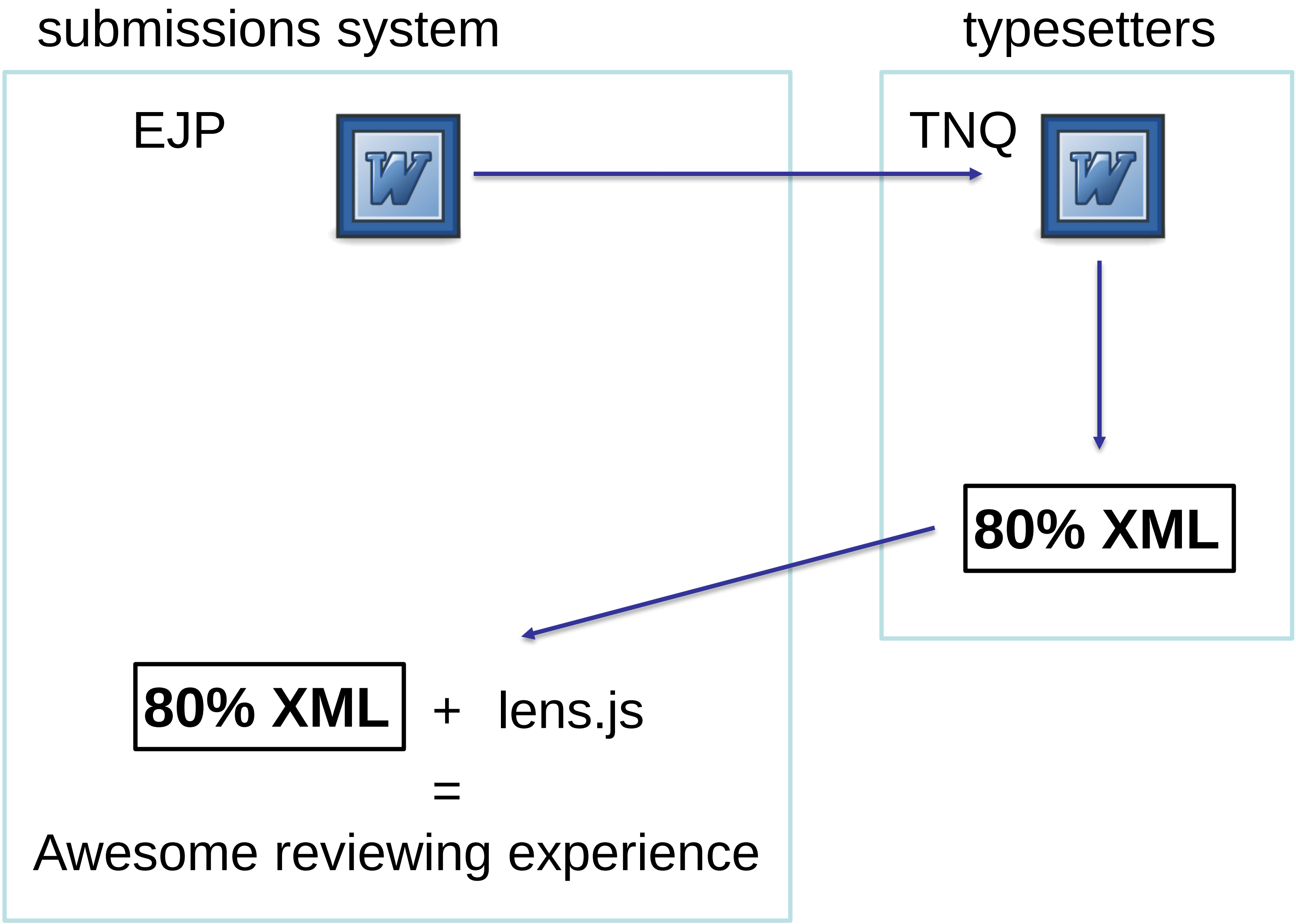
submissions system
typesetters
EJP
TNQ
80% XML
80% XML
+ lens.js
=
Awesome reviewing experience

stm

proteins were found to be involved in the multiple cellular process like transcription, telomerase core complex assembly, cell cycle progression, apoptosis, snoRNPs biogenesis, PIKK mediated signaling, RNA polymerase II assembly, as well as in the mitosis.[5-7] Recently human RuvB1 and RuvB2 are in the focus because of their involvement in many human cancers[8] like hepatocellular carcinomas,[9] renal and gastric carcinomas.[10] The biochemical characterization reports on RuvB like proteins established that these are active ATPase and many reports have also shown their helicase activity.[6] Due to the presence of ATPase activity and involvement in multiple cellular processes these proteins have been categorized as AAA+ proteins (ATPases associated with multiple cellular processes).

Pih1 is an unstable protein however stabilizes itself after interaction with Hsp90 and Tah1.[2] Pih1 interacts with snoRNPs factor Nop1/fibrillarin, Nop58, Tel2, Monad and play crucial role in snoRNPs biogenesis and PIKK signaling.[11] Tah1 is characterized as the cofactor of Hsp90 and enhances the activity of Hsp90 protein.[1] Human counterpart of Tah1 is known as RPAP3 which is almost 6 times bigger in terms of number of amino acid as well as in number of TPR repeat. Yeast Tah1 contains 2 TPR repeats while RPAP3 contains 6 TPR repeats.

R2TP complex has been found to play an important role in many processes like RNA polymerase-II assembly, snoRNPs assembly, PIKK signaling, and in the apoptosis.[11] R2TP-Hsp90 complex together with Perfoldin like complex interacts with RNA polymerase-II and was found to be crucial for the assembly of the RNA polymerase-II.[4] In yeast Pih1 deletion led disruption of R2TP complex resulted into decreased snoRNAs of box C/D.[2] Human RuvB1 and RuvB2 interact with almost all core box C/D snoRNPs factor and PIH1D1 directly interacts with Nop1, Nop58, and Nop56. RuvBs have been crucial for the box C/D and box H/ACA snoRNA.[12,13] The depletion of human RuvBL1 and RuvBL2 showed a decreased level of mature box C/D snoRNA,[14] thus providing the evidence of R2TP complex involvement in snoRNP assembly and biogenesis. Recently it has been discovered that R2TP complexes are also involved in the PIKK (phosphatidylinositol 3-kinase related protein kinase) signaling pathway.[15] RuvBL1 and RuvBL2

involvement in various activities was prepared on the basis of reported role in yeast and human. R2TP complex is involved in the diverse cellular activities shown in the figure.

Figure 2. Image mentioned 2 times

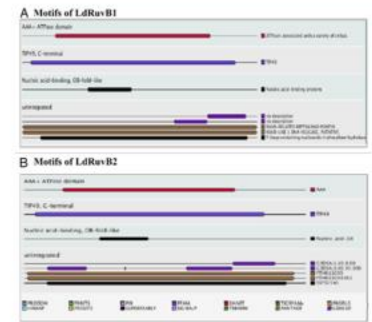

Figure 2. In-silico prediction of conserved motifs of RuvB from *L. donovani* using InterProScan. (**A**) Predicted motifs model of *L. donovani* RuvB1 was prepared, which

Landes Biosciences, PeerJ also interested are PLOS, Dove Press and a project from the University of California Davis

stm

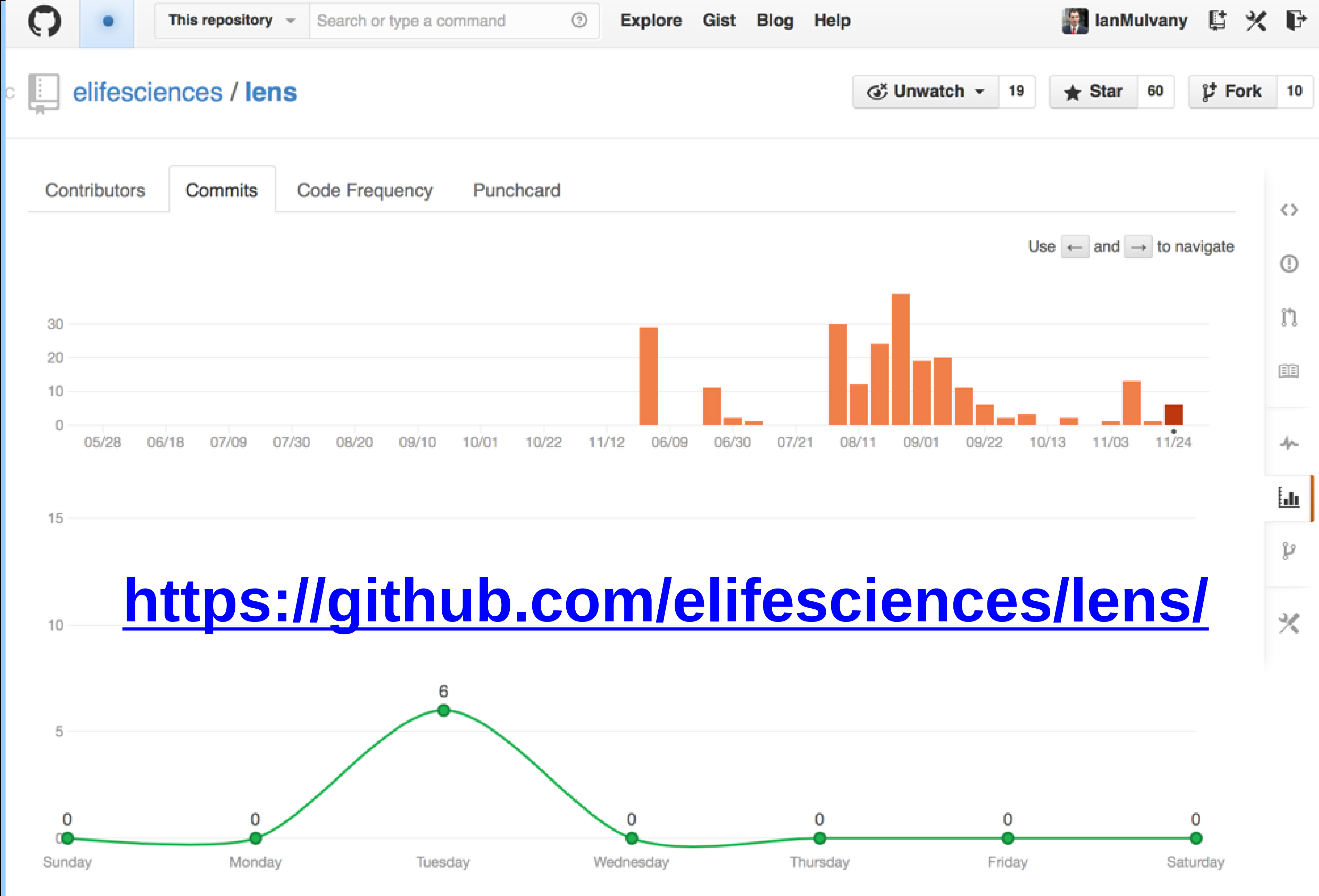

https://github.com/elifesciences/lens/

Altreader
Anableps
Glance
Kaleidoscope
Lens
Mix
Obake
Panorama
Panoreader
PaperView
Parallax
Quarto
Reader
Savvy
Scope
Sense
Spectare
Telescope
Vision
Visum
Wafer
eLluminate


lens.elifesciences.org
photo: cc-by via flickr: jordansorensen

Time’s Up!

About your speaker:

Name: Ian Mulvany

Company: eLife

Tel:

Email: i.mulvany@elifesciences.org

Social Media: @IanMulvany